[6] C. Zhang, J. Wang, S. Han, M. Yi, and Z. Zhang, "Automatic real-time barcode localization in complex scenes," in *IEEE Int. Conf. on Image Processing*, Oct. 8–11, 2006, pp. 497–500.
[7] C. Backstrom, C. Sodergard, and S. Udd, "A video processing method for convenient mobile reading of printed barcodes with camera phones," in *Proc. SPIE*, 2007, vol. 6073, pp. 1–12.
[8] S. M. Youssef and R. M. Salem, "Automated barcode recognition for smart identification and inspection automation," *Expert Syst. With Appl.*, vol. 33, pp. 968–977, 2007.
[9] D. Parikh and G. Jancke, "Localization and segmentation of a 2D high capacity color barcode," in *IEEE Workshop on Appl. of Computer Vision*, Jan. 2008, pp. 1–6.
[10] X. Liu, D. Doermann, and H. Li, "VCode-pervasive data transfer using video barcode," *IEEE Trans. Multimedia*, vol. 10, no. 3, pp. 361–371, Apr. 2008.
[11] H. Kato and K. T. Tan, "Pervasive 2D barcodes for camera phone applications," *IEEE Pervasive Comput.*, vol. 6, no. 4, pp. 76–85, Oct.–Dec. 2007.
[12] C. Chen, A. C. Kot, and H. Yang, "A quality measure of mobile phone captured 2D barcode images," in *2010 IEEE Int. Conf. on Image Process. (ICIP'2010)*, Hong Kong, Sep. 26–29, 2010, pp. 329–332.
[13] H. Yang, A. C. Kot, and X. Jiang, "Knowledge guided adaptive binarization for 2D barcode images captured by mobile phones," in *35th IEEE Int. Conf. on Acoust., Speech, Signal Process.(ICASSP'2010)*, Dallas, TX, Mar. 14–19, 2010, pp. 1046–1049.
[14] H. Yang, X. Jiang, and A. C. Kot, "Localization of four extreme corners for barcode images reading using mobile phones," in *2010 IEEE Int. Conf. on Image Process. (ICIP'2010)*, Hong Kong, Sep. 26–29, 2010, pp. 3897–3900.
[15] H. Yang, A. C. Kot, and X. Jiang, "Dynamic window construction for the binarization of barcode images captured by mobile phones," in *2010 IEEE Int. Conf. on Image Process. (ICIP' 2010)*, Hong Kong, Sept. 26–29, 2010, pp. 3001–3004.
[16] *Information Technology-Automatic Identification and Data Capture Techniques-PDF417 Bar Code Symbology Specification*, , 2006.
[17] Niblack, *An Introduction to Digital Image Processing*. Englewood Cliffs, NJ: Prentice-Hall, 1986, pp. 115–116.
[18] *BS ISO/IEC 18004: Information Technology-Automatic Identification and Data Capture Techniques-QR Code Bar Code Symbology Specification*, BS ISO/IEC 18004, 2005.
[19] Tasman Barcode Reader [Online]. Available: http://www.tasman.co.uk
[20] ClearImage Barcode Reader [Online]. Available: http://www.inliteresearch.com/homepage/products/tools.html
[21] N. Otsu, "A threshold selection method from gray-level histograms," *IEEE Trans. Syst., Man, Cybern.*, vol. SMC-9, no. 1, pp. 62–66, Jan./Feb. 1979.
[22] T. W. Ridler and S. Calvard, "Picture thresholding using an iterative selection method," *IEEE Trans. Syst., Man, Cybern.*, vol. SMC-8, no. 4, pp. 630–632, Jul./Aug. 1978.
[23] J. R. Parker, "Gray level thresholding in badly illuminated images," *IEEE Trans. Pattern Anal. Machine Intell.*, vol. 13, no. 8, pp. 813–819, Aug. 1991.
[24] R. Fisher, S. Perkins, A. Walker, and E. Wolfart, Adaptive Thresholding 2003 [Online]. Available: http://homepages.inf.ed.ac.uk/rbf/HIPR2/adpthrsh.htm
[25] J. Kittler and J. Illingworth, "Threshold selection based on a simple image statistic," *Computer Vision, Graphics, and Image Processing*, vol. 30, pp. 125–147, 1985.
[26] Zxing Barcode Decoder [Online]. Available: http://code.google.com/p/zxing

Fast Vanishing-Point Detection in Unstructured Environments

Peyman Moghadam, *Student Member, IEEE*, Janusz A. Starzyk, *Senior Member, IEEE*, and W. S. Wijesoma, *Member, IEEE*

***Abstract*—Vision-based road detection in unstructured environments is a challenging problem as there are hardly any discernible and invariant features that can characterize the road or its boundaries in such environments. However, a salient and consistent feature of most roads or tracks regardless of type of the environments is that their edges, boundaries, and even ruts and tire tracks left by previous vehicles on the path appear to converge into a single point known as the vanishing point. Hence, estimating this vanishing point plays a pivotal role in the determination of the direction of the road. In this paper, we propose a novel methodology based on image texture analysis for the fast estimation of the vanishing point in challenging and unstructured roads. The key attributes of the methodology consist of the optimal local dominant orientation method that uses joint activities of only four Gabor filters to precisely estimate the local dominant orientation at each pixel location in the image plane, the weighting of each pixel based on its dominant orientation, and an adaptive distance-based voting scheme for the estimation of the vanishing point. A series of quantitative and qualitative analyses are presented using natural data sets from the Defense Advanced Research Projects Agency Grand Challenge projects to demonstrate the effectiveness and the accuracy of the proposed methodology.**

***Index Terms*—Dominant texture orientation, Gabor filters, vanishing-point detection.**

I. Introduction

Over the past few decades, there has been extensive research in developing autonomous navigation system (ANS) for unmanned ground vehicles in either structured urban environments or unstructured off-road conditions. One of the crucial parts of the ANS is the road detection system, which is able to discriminate between road (traversable path) and nonroad (nontraversable path) regions. Most of the current road detection systems use vision sensors for road detection [1]. The majority of vision-based road detection methods in the literature are grouped into three main categories: edge-, region-, and texture-based methods. Edge-based methods reduce the road detection to the extraction of road boundaries or lane markings. These approaches are more appropriate for structured roads, where the well-painted lane markings or strong edge boundaries (i.e., curbs) are the distinct features of

Manuscript received October 08, 2010; revised March 19, 2011 and June 29, 2011; accepted June 30, 2011. Date of publication July 18, 2011; date of current version December 16, 2011. The associate editor coordinating the review of this manuscript and approving it for publication was Dr. A. G. Bors.

P. Moghadam is with the Department of Electrical and Electronic Engineering, Nanyang Technological University, Singapore 639798, and also with the Deutsche Telekom Laboratories, 10589 Berlin, Germany (e-mail: peym.mo@gmail.com).

J. A. Starzyk is with the School of Electrical Engineering and Computer Science, Ohio University, Athens, OH 45701 USA, and also with the Department of Applied Information Systems, University of Information Technology and Management, 35-225 Rzeszow, Poland (e-mail: starzyk@bobcat.ent.ohiou.edu).

W. S. Wijesoma is with the Department of Electrical and Electronic Engineering, Nanyang Technological University, Singapore 639798 (e-mail: eswwijesoma@ntu.edu.sg).

Color versions of one or more of the figures in this paper are available online at http://ieeexplore.ieee.org.

Digital Object Identifier 10.1109/TIP.2011.2162422

the road [1], while they may not perform well in unstructured environments. Region-based methods look for distinct characteristics (i.e., color and/or texture) over local neighborhoods in order to segment the scene to path and nonpath regions [2]. These methods are suitable for types of environments where there is at least one unique surface road feature to distinguish from the surroundings. They also assume that road surfaces belong to relatively homogenous regions such as in well-paved roads. However, in unstructured environments, there are various types of terrain covers (soil, grass, rock, etc.) with complex geometric characteristics, uncontrolled lighting, and weather conditions, which make distinguishing road regions from surroundings extremely difficult [3].

To overcome the shortcomings of current road detection methods, texture-based techniques have been proposed. Instead of looking for locally distinctive road cues, they search for a global road constraint to distinguish road direction [4]–[7]. Texture-based methods search for local oriented textures and then make them vote for the locations of the road's vanishing points. A location with maximum votes is considered as the vanishing point of the main road region. Furthermore, the direction of the road or the road boundaries can be extracted by the information of the vanishing-point location. This paper belongs to this group of methods.

This paper proposes a new vanishing-point estimation method for autonomous navigation systems in rough and unstructured types of road terrains. This paper is organized as follows: Section II describes related vanishing-point detection algorithms. In Section III, we introduce a novel optimal local dominant orientation method (OLDOM) based on joint activities of only four Gabor filters. Section IV presents a new voting scheme for robust vanishing-point estimation. In Section V, we evaluate the performance of the proposed vanishing-point detection algorithm. Finally, we summarize the results and draw conclusions in Section VI.

II. Related Work

A set of lines in the image plane that corresponds to a set of parallel surface lines in the 3-D world space converges to a common point in the image space known as a vanishing point. Vanishing points are widely used in a diverse range of computer vision applications such as 3-D interpretation. In general, a man-made environment has two or three vanishing points, which correspond to different sets of parallels lines of the architectural structures such as buildings and walls stretched in the vertical or horizontal direction.

However, in the context of the cross-country environments, regardless of types of the roads, a unique vanishing point associated with the most immediate straight road parts in the direction of the optical axis of the forward-looking cameras can be determined. The vanishing point plays an important role as a global constraint for detecting road direction, since all parallel border road lines, road edges, and even ruts and tire tracks left by previous vehicles on the road appear to converge into a single vanishing point [see Fig. 1(a)]. In the case of a curved road, a single vanishing point can be estimated along the tangent directions of the most immediate road regions [red dash lines in Fig. 1(b)] in front of the vehicle. By estimating the vanishing-point location, the direction of the road in front of the vehicle can be approximately determined. Later, this can be utilized for the autonomous vehicle steering [8].

Most of the existing vanishing-point detection algorithms rely on three steps [9]–[11]. The first step performs edge detection on the image in order to extract the most dominant edges such as road borders or lane markings. The next step is to determine if there are any line segments in the image. Once all the line segments are identified, a voting procedure is applied to find the intersections of the lines. The shortcoming of all these methods is that they are based on edge detection followed by line extraction, which may restrain the process of detecting the true vanishing points in unstructured road conditions where there are no apparent boundaries.

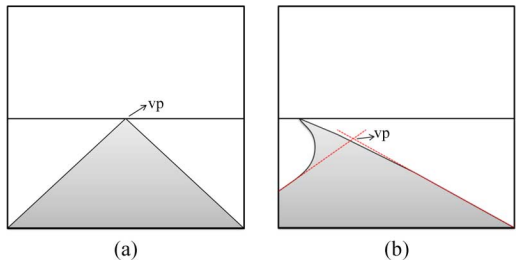

Fig. 1. Vanishing point (vp) in the (a) straight and (b) curved roads.

Aside from that, numerous vanishing-point detection methods have been proposed for man-made environments that do not depend on the edge detection step [12], [13]. These approaches search for similar global structures and repeating patterns (e.g., walls, doors, and windows) in the image to define the vanishing-point locations. However, it is unlikely that one can identify such repeating structures in outdoor unstructured environments.

To address the aforementioned drawbacks, Rasmussen [4] proposed texture-based methods to replace the noise-sensitive edge detection step of vanishing-point detection algorithms. Texture-based approaches apply a bank of oriented filters such as Gabor filter banks [4]–[6] or steerable filter banks [7], [14] and choose the orientation corresponding to the maximum filter response as the dominant texture orientation $\hat{\theta}(p)$ at each pixel location $p(x, y)$. Later, each local dominant orientation votes for the location of road's vanishing points. A location with maximum votes is considered as the vanishing point of the road.

However, in order to achieve precise orientation estimation, one needs to apply a large number of oriented filters in all possible directions from 0° to 180°. Designing and applying a bank of differently rotated filters is computationally expensive. To address this problem, Freeman and Adelson [15] proposed a steerable filter in which each arbitrary oriented filter can be formed by a linear combination of a fixed set of basis-oriented filters. Although the steerable filter is a more efficient approach compared with the bank of oriented filters, it still requires steering the basis-oriented filters in all orientations with a precise angle step size (e.g., 1° interval) and studying the outputs of the filters as a function of their orientations to find the maximum response as the local dominant orientation. To overcome the drawbacks of the existing texture-based vanishing-point detection methods, we propose a novel solution to directly estimate the local dominant orientation based on the joint activity of four Gabor filters with orientations $\{0^\circ, 45^\circ, 90^\circ, 135^\circ\}$ followed by an efficient and robust voting scheme suitable for real-time applications.

III. Local Dominant Orientation Estimation

In this paper, we use Gabor filters to estimate local dominant orientation at each pixel location. A 2-D Gabor kernel g for a preferred orientation φ_n and radial frequency $w_0 = 2\pi/\lambda$ [16] can be written as

$$g_{w_0,\varphi_n}(x, y) = \frac{w_0}{\sqrt{2\pi}K} e^{-\frac{w_0^2}{8K^2}(4a^2+b^2)} \cdot \left[e^{iw_0 a} - e^{-\frac{K^2}{2}} \right] \quad (1)$$

where $a = x\cos\varphi_n + y\sin\varphi_n$, $b = -x\sin\varphi_n + y\cos\varphi_n$, $K = \pi/2$ is a constant, and the spatial frequency λ is set to $4\sqrt{2}$. In order to estimate the dominant orientation $\theta(p)$ at each pixel location $p(x, y)$

in the image, the grayscale input image $I(p)$ is convolved with a bank of Gabor filters with predefined orientations, i.e.,

$$\hat{I}_{\varphi n}(p) = I(p) \otimes g_{\varphi_n}(p)$$
$$\varphi_n = \frac{(n-1)\pi}{N_\varphi} \qquad n = 1, 2, \ldots, N_\varphi \tag{2}$$

where $\otimes$ denotes the convolution operator and N_φ is the total number of orientations. Finally, the Gabor energy $E_{\varphi_n}(p)$ is calculated as the magnitude of the complex filter response as follows:

$$E_{\varphi_n}(p) = \sqrt{\mathrm{Re}\left(I_{\varphi_n}(p)\right)^2 + \mathrm{Im}\left(\hat{I}_{\varphi_n}(p)\right)^2}. \tag{3}$$

The orientation corresponding to the strongest Gabor energy response across all orientations at each pixel location is chosen as the local dominant texture orientation. Almost all the local texture orientation estimation methods use a bank of Gabor filters with a large number of orientations to achieve a precise angular resolution for the local dominant orientation $\theta(p)$ ($N_\varphi = 72$ in [4] and $N_\varphi = 36$ in [5], [6]). Therefore, in order to overcome this drawback of the existing texture orientation detection methods, we propose a novel OLDOM to estimate the dominant orientation as described next.

A. Optimal Local Dominant Orientation Method

Every vector in R^2 can be represented by a unique combination of two linearly independent vectors. Hence, every local texture orientation in the image represented by a vector can be obtained by using only two independent Gabor energy filter responses, which strongly respond to that texture vector orientation. More specifically, to estimate the dominant orientation $\theta(p)$ at each pixel location $p(x, y)$ in the image, an input grayscale image is convolved with four oriented Gabor filters g_φ, $\varphi \in \{0^\circ, 45^\circ, 90^\circ, 135^\circ\}$, and Gabor energy responses are computed for each pixel location. Each Gabor energy response is considered as a vector whose magnitude is proportional to the Gabor energy response value $E_\varphi(p)$ and its direction corresponds to its preferred orientation φ. Next, these Gabor energy responses $E_\varphi(p)$ are sorted based on their magnitudes in descending order ($E^1_\varphi(p) > E^2_\varphi(p) > E^3_\varphi(p) > E^4_\varphi(p)$) for each pixel location $p(x, y)$. Then, the resulting vector $\mathbf{V}$ of the two most dominant filter activation strengths will be used to represent the local texture orientation as follows:

$$\mathbf{V}(p) = V_x(p) + \mathrm{j}V_y(p) = \sum_{i=1}^{2} E^i_\varphi(p) e^{j\varphi_i} \tag{4}$$

where φ_1 and φ_2 represent the angle of the two dominant Gabor energy responses $E^1_\varphi(p)$ and $E^2_\varphi(p)$, respectively. Next, the estimated dominant orientation $\hat{\theta}(p)$ at pixel p is determined by

$$\hat{\theta}(p) = \tan^{-1}\frac{V_y(p)}{V_x(p)}. \tag{5}$$

However, if the pixel is related to a feature in the image with no apparent dominant orientation, which often appears in cluttered nonroad regions, the Gabor energy response values may be very similar for all four orientations. In such a case, relying only on the two strongest filter responses may result in a large estimation error of the dominant orientation $\theta(p)$. To solve this problem, we propose to use joint activities of all four Gabor energy responses by introducing two new vectors $S_1(p)$ and $S_2(p)$ defined as follows:

$$\begin{cases} \|S_1(p)\| = E^1_\varphi(p) - E^4_\varphi(p) \\ \varphi_{S1}(p) = \varphi_1(p) \end{cases} \tag{6}$$

$$\begin{cases} \|S_2(p)\| = E^2_\varphi(p) - E^3_\varphi(p) \\ \varphi_{S2}(p) = \varphi_2(p) \end{cases} \tag{7}$$

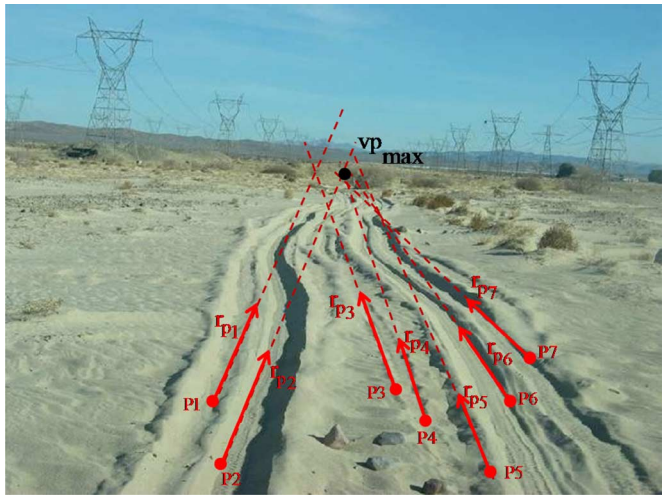

Fig. 2. Upward voting. Candidate vanishing-point $\mathrm{vp}_{\max}$ is receiving supports from possible texture orientations voters.

where φ_{S_1} and φ_{S_2} represent the angle of two new vectors $S_1(p)$ and $S_2(p)$, respectively. Then, (4) can be replaced by these two new vectors as follows:

$$\mathbf{V}(p) = \sum_{i=1}^{2} S_i(p) e^{j\varphi_{S_i}}. \tag{8}$$

Next, the local dominant orientation at pixel location $p(x, y)$ can be defined by (5). Therefore, the proposed OLDOM estimates the local dominant orientation based on the joint activity of only four Gabor filters. In Section V, we evaluate the accuracy of the proposed OLDOM method.

IV. Vanishing Point Voting

Once the dominant orientation $\hat{\theta}(p)$ is estimated at each pixel location $p(x, y)$ of the image, a ray defined by $r_p = (p, \hat{\theta}(p))$ is drawn upward in an accumulator space, which has the same size as the input image. The accumulator space of all pixels is initialized to zero. If a pixel lies on ray r_p, it gets incremented by 1 provided that it is located above point $p(x, y)$. After rendering all the rays, a pixel with the maximum number of supporting rays is declared as the candidate vanishing point $\mathrm{vp}_{\max}$ [5]. Fig. 2 demonstrates an example of the candidate vanishing point $\mathrm{vp}_{\max}$ with supporting texture orientations voting for its location.

A. Weighting Method

In the conventional voting methods [4], [5], all the dominant orientations that come either from the strong edges of the road or from any random off-road region have the same influence on the voting scheme. Therefore, it may lead to incorrect estimation of the vanishing-point location. To resolve this effect, we propose to assign a weight to each ray r_p based on the trigonometric function of its dominant orientation ($\sin\hat{\theta}(p)$). The reason is that the vanishing point is expected to be mostly determined by supporting rays with a range of angles closer to vertical orientations than horizontal ones. Therefore, by weighting each dominant orientation by its sine function, those horizontal or nearly horizontal orientations are suppressed.

B. Voting Scheme

Although the proposed weighting method resolves the problem of assigning a weight to each ray r_p, since it allows only pixels to vote upward, it is biased toward higher pixels in the image [4]. Hence, the

pixels in the upper part of the image receive more votes than lower image pixels. In order to overcome the biases to effectively estimate the vanishing-point location, we propose a new distance-based voting scheme.

This approach implies that each dominant orientation gives higher vote to the points closer to it than to the points further away along its ray r_p. We define a function based on the normalized Euclidean distance between each dominant orientation location $p(x, y)$ and each point on its ray r_p. The distance value is first normalized by the maximum possible distance D_p between pixel $p(x, y)$ and the intersection point of its ray with the image perimeters (depends on the angle of its orientation).

Then, the distance function $y_j(\hat{d})$ is computed as

$$y_j(\hat{d}) = e^{-\frac{\hat{d}^2}{2\sigma^2}} \quad \hat{d} = \frac{d}{D_p} \quad d = \sqrt{(x - x_j)^2 + (y - y_j)^2} \tag{9}$$

where $y_j(\hat{d})$ is the distance function, d is the distance between the dominant orientation $p(x, y)$ and any point (x_j, y_j) on its ray r_p, $\hat{d}$ is the normalized distance, and σ^2 is the variance that is experimentally set to 0.25. Consequently, each ray r_p with dominant estimated orientation $\hat{\theta}(p)$ is first weighted based on the sine function of its dominant orientations $(\sin \hat{\theta}(p))$, and then, it is multiplied by the distance function $y_j(\hat{d})$ to give a higher vote to the points closer to its origin than to the points further away along ray r_p.

V. Results and Analysis

First, to assess the accuracy of the proposed OLDOM, a set of synthetic images with associated ground-truth orientations are generated. Each image contains a white line with an intensity of 255 in a black (zero-intensity) background. Each line crosses the center of the image by a set angle ranging from 0° to 180° with a step size of 1°. Four oriented Gabor filters $\{0^\circ, 45^\circ, 90^\circ, 135^\circ\}$ are applied to each pixel location of the input image, and Gabor energy responses are calculated at ten randomly selected points scattered from the center along each line. The mean and the standard deviation of the estimated texture orientations for these ten points are measured and compared with the ground truth. The error is calculated based on the difference between the actual ground-truth orientation and the estimated orientation in degrees. The results indicate that the proposed technique has a finite angular resolution of 1.4° ($\pm 0.75^\circ$). Such accuracy would require 128 evenly spaced oriented filters from 0° to 180° in the conventional bank of oriented filters methods [4]–[7].

Next, to determine the quality of our vanishing-point estimation in unstructured environments, we conducted experiments with images from unstructured and cross-country conditions. The data set used for the evaluation of the proposed vanishing-point detection consists of 500 natural images from a set of digital photographs taken on a scouting trip along a Grand Challenge route in the Mojave Desert [3]. The data set contains various types of ground covers (soil, rock, etc.) with complex geometric characteristics, different illuminations and weather conditions, and shadows. All the images are rectified and undistorted with the size of 320×240 and taken by a forward-looking camera mounted in front of the vehicle.

A. Performance Metric

The vanishing-point estimation error was measured by comparing the result of the algorithms against the vanishing-point ground truth manually determined through human perspective perception [4]–[6]. We invited 20 participants from our department to manually mark the vanishing-point location in each image of the data set after a brief description of the road vanishing-point concept. We assumed the distribution of the users' marked points is Gaussian, and we defined the center as the ground-truth vanishing-point location.

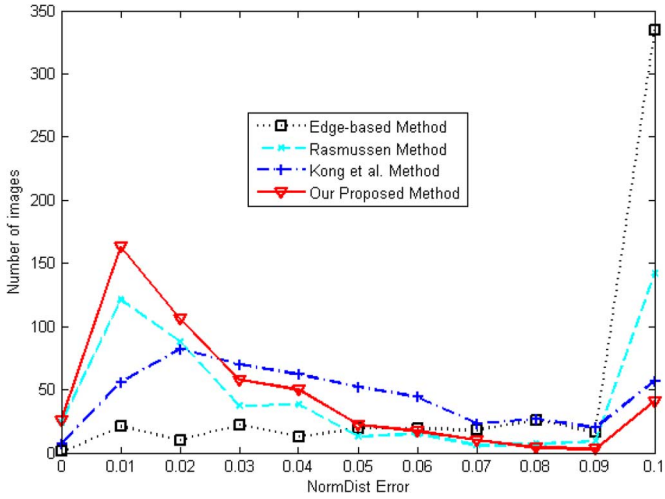

Fig. 3. Comparison of vanishing-point detection methods in an 11-bin histogram.

TABLE I
Accuracy Comparison

	Edge-based method [11]	Rasmussen [5]	Kong et al. [6]	Our proposed method
Error (NormDist)	0.1710	0.0903	0.052	**0.036**

To measure the vanishing-point estimation error, previous methods either determine pixel difference between the estimated vanishing-point location and the ground truth separately in both column and row [4] or use one metric such as the Euclidean distance in pixels [6] to show the quality of the vanishing-point estimation. However, when different methods have different image resolutions, the error in pixels is not a representative of the true performance of different methods. For quantitative evaluation measurements, we suggest to use the normalized Euclidean distance, where the Euclidean distance is normalized by the size of the diagonal of the image resolution as follows:

$$\text{NormDist} = \frac{\|P - P_0\|}{\text{Diag Image}} \tag{10}$$

where $P(x_p, y_p)$ is the estimated vanishing-point location and $P_0(x_0, y_0)$ is the center of the ground-truth vanishing-point location, while "Diag Image" is the size of the diagonal of the image. Using the proposed metric, a value near 1 would correspond to the incorrectly estimated vanishing-point location. A value near 0 means that the estimated vanishing-point location is close to the location of the ground truth.

B. Experimental Results

Here, we evaluate the performance of the proposed vanishing-point method both quantitatively and qualitatively. In order to decrease the computational demand to meet the real-time requirements for ANS applications, all the images in the data set are first downsized to 80×60 pixels by the Gaussian pyramid and then passed to the vanishing-point detection method to find the vanishing-point location. Once the van-

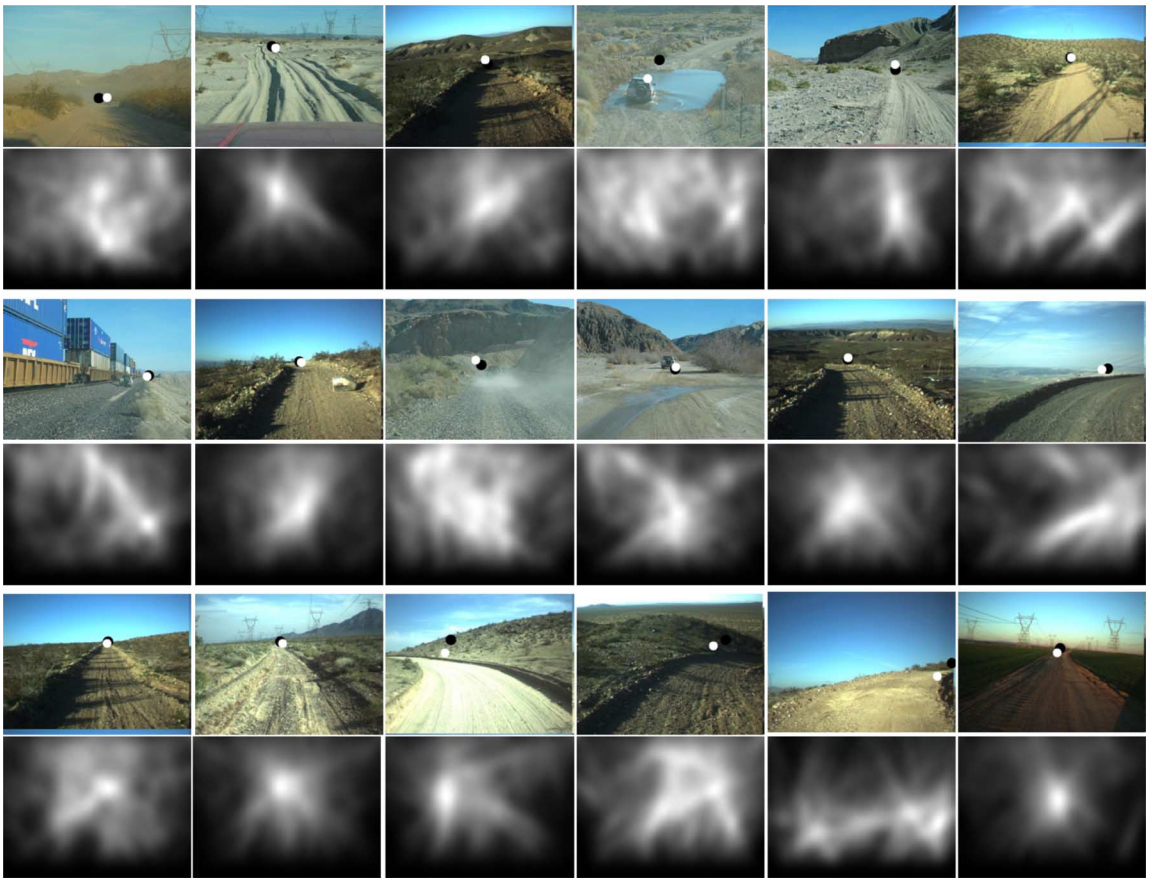

Fig. 4. Examples of vanishing-point detection for unstructured roads. First, third, and fifth row: outputs of this paper's algorithm (black dot is the ground truth and white dot is the estimated vanishing-point location); second, fourth and sixth row: accumulator spaces.

ishing-point location is estimated in the downscaled image, its location is projected back to the original image size (320 × 240) to assess the algorithm's performance with the human-perception ground truth.

For quantitative comparison purposes, we evaluated the proposed method results relative to the classical edge-based (Canny/Hough) vanishing-point detection method [11] and the two best known texture-based vanishing-point detection algorithms for unstructured and off-road conditions proposed in [5] and [6]. Table I shows the numerical results in terms of the average normalized Euclidean distance error for the data set. As shown in the Table I, our proposed method outperforms all vanishing-point detection algorithms significantly. As we expected, the edge-based method is not suitable for clutter unstructured environments, where there is no clear edges and apparent parallel lines to extract. For in-depth analysis and better comparison, we also evaluated the results of our proposed method versus the edge-based method [11], the Rasmussen method [5], and the Kong *et al.* method [6] in an 11-bin histogram. We consider the distance of 0.1 as a very large error, therefore, if the normalized Euclidean distance between the estimated vanishing-point location and the ground truth is larger than or equal to 0.1, it is placed into the last histogram bin, as shown in Fig. 3. The vertical axis shows the number of images in each histogram bin, and the horizontal axis shows the normalized distance error (NormDist). A larger number of images in the left part of the histogram depict better results, whereas the larger values in the right part show worse cases.

The advantage of our proposed method is that it has the greatest number of images in the left part of the histogram (i.e., low error rate) with the smallest number of images with large errors at the right side of the histogram.

In particular, in the Rasmussen method [5], error rates of more than 142 images (28%) are greater than 0.1, whereas in our proposed method, it is only less than 41 images (8%). Aside from that, the Kong *et al.* method [6] shows 56 (11%) images with large error, which is better than the Rasmussen method [5], while its performance is degraded in the small error portions of the histogram (i.e., left part). The NormDist error less than 0.01 in the Kong *et al.* method [6] occurs in only 63 (12%) images. In contrast, our proposed method performs significantly better in which 189 images (37%) have the normalized distance error (NormDist) of less than 0.01. Moreover, the edge-based method [11] shows the worst results compared with texture-based methods, where over 335 images (67%) have the error greater than 0.1.

Fig. 4 depicts a variety of images with estimated vanishing points overlaid on the images showing that our proposed method estimates the vanishing-point locations successfully in many challenging unstructured roads and illumination conditions. Note that, in curved roads, the main vanishing point associated with the tangent directions of the most immediate road regions in front of the vehicle is correctly estimated.

Although the algorithm is proposed for off-road unstructured environments, it works perfectly well for structured road conditions (straight or curved). In structured roads, many supporting oriented texture cues such as well-painted lane markings or strong edge boundaries point to the candidate vanishing points. Fig. 5 illustrates examples of applying our proposed method to structured road conditions. As demonstrated, the proposed method accurately estimates the vanishing point in structured environments as well. The estimation is even more accurate for such structured road conditions.

Fig. 5. Examples of vanishing-point detection for structured roads. First and third row: outputs of this paper's algorithm (black dot is the ground truth and white dot is the estimated vanishing-point location); second and fourth row: accumulator spaces.

VI. Conclusion

We have proposed a new vanishing-point estimation method for outdoor unstructured road conditions. The technique relies on the joint activities of four Gabor filters in order to estimate the dominant orientation at each pixel location in the image robustly, thereby making it ideally suitable for real-time applications. After the dominant orientation has been estimated, in order to locate the vanishing point, a novel voting method has been presented, which assigns an adaptive weight to each ray drawn along a dominant orientation. Those weighted rays are further enhanced by the distance-based voting scheme to overcome the biases toward the higher pixels in the image. Finally, the pixel with the maximum supporting rays is declared as the candidate vanishing point of the main portion of the road. Furthermore, a series of quantitative and qualitative analyses have been conducted using natural data sets from the Defense Advanced Research Projects Agency project. The performance in terms of accuracy of the proposed method outperforms the state-of-the-art vanishing-point detection methods.

References

[1] C. Thorpe, M. Hebert, T. Kanade, and S. Shafer, "Vision and navigation for the Carnegie-Mellon Navlab," *IEEE Trans. Pattern Anal. Mach. Intell.*, vol. 10, no. 3, pp. 362–373, May 1988.

[2] Y. Alon, A. Ferencz, and A. Shashua, "Off-road path following using region classification and geometric projection constraints," in *Proc. IEEE Conf. Comput. Vis. Pattern Recog.*, 2006, pp. 689–696.

[3] S. Thrun, M. Montemerlo, H. Dahlkamp, D. Stavens, A. Aron, J. Diebel, P. Fong, J. Gale, M. Halpenny, and G. Hoffmann, "Stanley: The robot that won the DARPA grand challenge," *J. Field Robot.*, vol. 23, no. 9, pp. 661–692, Sep. 2006.

[4] C. Rasmussen, "Grouping dominant orientations for ill-structured road following," in *Proc. IEEE Conf. Comput. Vis. Pattern Recog.*, 2004, pp. 470–477.

[5] C. Rasmussen, "RoadCompass: Following rural roads with vision + ladar using vanishing point tracking," *Auton. Robots*, vol. 25, no. 3, pp. 205–229, Oct. 2008.

[6] H. Kong, J. Audibert, and J. Ponce, "General road detection from a single image," *IEEE Trans. Image Process.*, vol. 19, no. 8, pp. 2211–2220, Aug. 2010.

[7] M. Nieto and L. Salgado, "Real-time vanishing point estimation in road sequences using adaptive steerable filter banks," in *Proc. ACIVS*, 2007, pp. 840–848.

[8] R. Schuster, N. Ansari, and A. Bani-Hashemi, "Steering a robot with vanishing points," *IEEE Trans. Robot. Autom.*, vol. 9, no. 4, pp. 491–498, Aug. 1993.

[9] T. Suttorp and T. Bucher, "Robust vanishing point estimation for driver assistance," in *Proc. IEEE Intell. Transp. Syst. Conf.*, 2006, pp. 1550–1555.

[10] T. Tuytelaars, L. Van Gool, M. Proesmans, and T. Moons, "The cascaded Hough transform as an aid in aerial image interpretation," in *Proc. 6th Int. Conf. Comput. Vis.*, 1998, pp. 67–72.

[11] Y. Wang, E. K. Teoh, and D. Shen, "Lane detection and tracking using B-Snake," *Image Vis. Comput.*, vol. 22, no. 4, pp. 269–280, Apr. 2004.

[12] H. Kogan, R. Maurer, and R. Keshet, "Vanishing points estimation by self-similarity," in *Proc. IEEE Conf. Comput. Vis. Pattern Recog.*, 2009, pp. 755–761.

[13] F. Stentiford, "Attention-based vanishing point detection," in *Proc. IEEE Int. Conf. Image Process.*, 2007, pp. 417–420.

[14] J. C. McCall and M. M. Trivedi, "Video-based lane estimation and tracking for driver assistance: Survey, system, and evaluation," *IEEE Trans. Intell. Transp. Syst.*, vol. 7, no. 1, pp. 20–37, Mar. 2006.

[15] W. T. Freeman and E. H. Adelson, "The design and use of steerable filters," *IEEE Trans. Pattern Anal. Mach. Intell.*, vol. 13, no. 9, pp. 891–906, Sep. 1991.

[16] T. Lee, "Image representation using 2D Gabor wavelets," *IEEE Trans. Pattern Anal. Mach. Intell.*, vol. 18, no. 10, pp. 959–971, Oct. 1996.